DOI: 10.1002/cjoc.201500248

Morphology-Tunable Fluorescent Nanoparticles: Synthesis, Photophysical Properties and Two-Photon Cell Imaging

Xiaoming Hu,[†,a] Chao Yin,[†,a] Wenbo Hu,[a] Zhen Yang,[a] Jie Li,[a] Xiang Li,[a] Xiaomei Lu,[a,b] Hui Zhao,[a] Yufu Tang,[a] Quli Fan,[*,a] and Wei Huang[*,a,b]

[a] *Key Laboratory for Organic Electronics and Information Displays & Institute of Advanced Materials, Jiangsu National Synergetic Innovation Center for Advanced Materials, Nanjing University of Posts & Telecommunications, Nanjing, Jiangsu 210023, China*

[b] *Key Laboratory of Flexible Electronics & Institute of Advanced Materials, Jiangsu National Synergetic Innovation Center for Advanced Materials, Nanjing Tech University, Nanjing, Jiangsu 211816, China*

A novel water-soluble fluorescent amphiphile based on amino polyethylene glycol (PEG-NH_2) substituted oligo(*p*-phenyleneethynylene) (OPE) was designed and synthesized successfully. Taking anion OPE amphiphile as a comparison, the photophysical features were investigated through ultraviolet absorption (UV) and photoluminescence (PL) analyses. Due to the hydrophobic-hydrophilic property of the OPE conjugated molecule, self-assembled nanoparticles with the size ranging from 19.6 to 93.5 nm along with the change of morphology from "grain" to "strawberry" were conveniently prepared via adjusting concentrations of OPE aqueous solution. Interestingly, after aging for a period of time, homogeneous hollow nanospheres were spontaneously constructed with a diameter of about 200 nm. Cytotoxicity test and cellular uptake behavior of the nanoparticles were further investigated to evaluate their potential biomedical applications. Subsequently, the promising applications of two-photon cell imaging were explored using human pancreatic cancer cells (PANC-1 cells), which indicated that the nanoparticles were mainly located within the cell cytoplasm.

Keywords water-soluble fluorescent nanoparticles, oligo(*p*-phenyleneethynylene) amphiphile, hollow nanospheres, two-photon cell imaging

Introduction

Recent years have witnessed the rapid development of water-soluble fluorescent π-conjugated oligomers/polymers and their various bioapplications, including highly efficient chemosensors or biosensors,[1-4] optical imaging *in vitro* and *in vivo*,[5] gene delivery,[6] drug screening, anticancer therapy[5] and so on. A new useful characteristic of water-soluble conjugated oligomers or polymers is their potential ability to form nanoparticles (NPs), which present great potential in biological imaging and drug delivery[7] applications for their superior features, such as facile chemical synthesis,[8] excellent photostability,[9] high brightness,[10] tunable photoluminescent properties,[11] and versatile surface modification.[12] For this, three approaches are usually adopted to prepare conjugated polymer nanoparticles. In the first approach, water-soluble fluorescent nanoparticles were constructed from hydrophobic conjugated polymers/oligomers and water-soluble polymers (such as poly(ethylene glycol), poly(galactose) and poly(acrylic acid))[13] or amphiphilic molecules (such as phospholipids and DSPE-PEG)[14] through noncovalent bond self-assembly. The second approach is transferring oil-soluble conjugated polymers into water dispersed conjugated polymer dots (CPdots) which show relatively steady fuorescence and ultrahigh brightness through a reprecipitation method.[15] As for the third approach, amphiphilic conjugated polymers are directly dispersed in a selective solvent to form various well-defined supramolecular architectures, such as micelles and vesicles,[16] which provide wide application in chemistry, biology, and materials science.[17] Compared with the first two approaches, this is an exactly fast and facile method to fabricate water-soluble conjugated polymer nanoparticles. For example, homogeneous nanoparticles were obtained through self-assembly using amphiphilic hyperbranched conjugated polyelectrolytes possessing hydrophobic PF internal cores and hydrophilic PEG external shells and their live cell imaging was further investigated by Liu and co-workers.[18,19]

However, applications in biological system of these

* E-mail: iamqlfan@njupt.edu.cn, wei-huang@njtech.edu.cn; Tel.: 0086-025-85866396; Fax: 0086-025-85866533; † Xiaoming Hu and Chao Yin are the co-first authors.
Received March 27, 2015; accepted May 27, 2015; published online July 22, 2015.
Supporting information for this article is available on the WWW under http://dx.doi.org/10.1002/cjoc.201500248 or from the author.

robust nanomaterials are usually hampered by the losing tunability of their morphology and size due to polymers' amorphous character and large molecular weight.[20] Thus, lots of efforts have been made to solve these problems such as changing solvent environments,[11] adjusting molecular structures and shapes,[21-23] as well as the control of relative proportion of hydrophilic and hydrophobic parts.[24] Yet, all the methods abovementioned are not very facile and controllable in practice, which still makes it complex to tune the morphology and size of nanostructures precisely. Therefore, the development of novel water-soluble conjugated polymer nanoparticles with morphological tunability, good biocompatibility, and excellent photoelectric features for bioimaging and biosensing is highly desired.

Here, a novel amphiphilic oligomer consisting of oligo(*p*-phenyleneethynylene) (OPE) and amino polyethylene glycol (PEG-NH_2) was designed and synthesized, and the photophysical properties, controllable self-assembly behaviors and two-photon cell imaging were further investigated. The employment of OPE and PEG stems from high quantum yields and photostability of OPE chromophore,[25] and prominent biocompatibility of PEG chains. Due to the hydrophobic-hydrophilic property of the OPE conjugated molecule, it can spontaneously aggregate to form nano-clusters ranging from 19.6 to 93.5 nm along with the morphological conversion from "grain" to "strawberry" just by controlling concentrations of OPE aqueous solution (from 0.0642 to 0.2168 mg/mL). More interestingly, after the solution was aged for one week at room temperature, homogeneous hollow nanospheres with a diameter of about 200 nm were obtained easily. All these provided a facile and convenient access to tuning the morphology and size of water-soluble fluorescent nanoparticles. The morphology and size of nanoparticles were characterized by transmission electron microscopy (TEM) and dynamic light scattering (DLS), respectively. Besides, ^{1}H NMR and Zeta potential confirmed the existence of amino groups on particle surface, which can be available for the subsequent modification. Furthermore, cytotoxicity test and cellular uptake behavior were investigated to confirm excellent biocompatibility of the OPE nanoparticles. Based on these, two-photon excited live cell imaging was conducted with confocal laser scanning microscopy, which presented strong fluorescence from cellular cytoplasm with considerably high contrast and spatial resolution. Due to the unique hollow structure of obtained nanospheres, they may become carrier of drugs and the template for fabricating multifunctional nanoprobes for biological application.

Experimental

General methods

All NMR spectra were recorded on a Bruker Ultra Shield Plus 400 MHz NMR at 22 ℃ and tetramethylsilane was used as internal reference. GC-MS was determined on a Shimadzu GC-MS-QP 2010 Plus mass spectrometer. Matrix assistant laser desorption/ionization time-of-flight mass spectrometry (MALDI-TOF-MASS) was measured on Bruker autoflex under the reflector mode for data acquisition. Gel permeation chromatography (GPC) results were obtained with Shimadzu LC-VP system with polystyrenes as the standard and high purity of THF as the eluent. The UV-Vis absorption and PL emission spectra were recorded on Shimadzu UV-3600 and RF-5301PC spectrometers, respectively. FT-IR spectra were recorded with a Shimadzu IR Affinity-1 spectrometer by dispersing samples in KBr. Morphological characterization of nanoparticles was conducted using fluorescence microscopy (Olympus IX71) and low resolution transmission electron microscope (TEM) (JEOL JEM-2100 transmission electron microscope operating at an acceleration voltage of 100.0 kV). Dynamic light scattering (DLS) and Zeta potential results were obtained with Brookhaven system. Two-photon fluorescence microscopy (2PFM) images in PANC-1 cells were collected on a modified Olympus Fluoview (FV1000) microscope system coupled to a Coherent MIRA Ti: sapphire laser, which was used for two-photon absorption measurements.

Cytotoxicity test

The cytotoxicity of the amphiphilic oligomer was evaluated by determining the viability of human pancreatic cancer cells (PANC-1) after incubation with DMEM containing our amphiphilic material at a variety of concentrations from 0.0001 to 0.5 mg/mL. Cell viability testing was carried out via the reduction of the MTT reagent. PANC-1 cells were seeded at a density of 10^4 cells per well for 24 h before the medium was replaced with one containing amphiphilic oligomer at different concentrations. Then the cells were incubated at 37 ℃ with 5% CO_2 for 24 h. After the designated time intervals, the wells were washed twice with PBS buffer and freshly prepared MTT (10 μL, 5 mg/mL in PBS) solution in a culture medium was added into each well. The MTT medium solution was carefully removed after 3 h incubation in the incubator. After that, DMSO (150 μL) was then added into each well and the wells were gently shaken for 10—20 min at room temperature to dissolve all the precipitate formed. The optical absorbance was then measured at 490 nm on a microplate reader (Tecan GENios). Cell viability was expressed by the ratio of the absorbance of the cells incubated with the amphiphilic oligomer solution. Each result is an average of data from six wells and the standard deviation was also calculated. 100% cell viability was determined using untreated cells.

Live cell imaging

PANC-1 cells were first seeded into confocal microscope dishes at 5×10^5/mL in complete DMEM medium and cultured for 24 h at 37 ℃. The medium was then replaced by DMEM medium with OPE nanoparticles

solution (0.2168 mg/mL). After incubation for 24 h at 37 ℃, the cells were rinsed three times with PBS buffer. 2PFM images in PANC-1 cells were collected on a modified Olympus Fluoview (FV1000) microscope system.

Synthesis

The OPE amphiphile (**4**) was synthesized by the route shown in Scheme 1. First, **1** was prepared according to the previous report[14] with a yield of 77.25% [^{1}H NMR ($CDCl_3$) δ: 7.35 (d, J=9.2 Hz, 2H), 6.78 (d, J=9.2 Hz, 2H), 3.91 (t, J=6.8 Hz, 2H), 1.73−1.80 (m, 2H), 1.26 (s, 18H), 0.88 (t, J=7.2 Hz, 3H). GC-MS (m/z): 340 (M^+)]. Then, **2** was synthesized based on the Pd-catalyzed Sonogashira reaction by "one-pot" approach: 4.68 g (13.73 mmol) of **1**, 1.73 g (13.73 mmol) of 1,4-diethynylbenzene, 3.75 g (13.73 mmol) of dimethyl 5-bromoisophthalate, 0.795 g (0.687 mmol) of $Pd(PPh_3)_4$ and 0.132 g (0.693 mmol) of CuI were poured into a 250 mL round-bottom flask with magnetic stirring bar and reflux condenser under dark condition. Then 120 mL diisopropylamine was injected into the round-bottom flask under nitrogen protection. And the mixture was stirred at 85 ℃ for 24 h. The product was then purified as a light yellow solid (2.16 g, yield 27.22%) through silica gel eluting with PE/DCM=3/1 [^{1}H NMR ($CDCl_3$) δ: 8.63 (s, 1H), 8.37 (s, 2H), 7.45−7.51 (m, 6H), 6.89 (d, J=8.8 Hz, 2H), 3.95−3.99 (m, 8H), 1.76−1.82 (m, 2H), 1.26 (s, 18H), 0.88 (t, J=7.2 Hz, 3H). GC-MS (m/z): 578 (M^+)]. Subsequently, all of the products (**2**) obtained above were dissolved in 30 mL THF, and a hydrolysis reaction under 65 ℃ for 5 h with KOH (3.0 g) and tetrabutyl ammonium bromide (0.8 g) was conducted. After the residual THF was removed by rotary evaporation, excess hydrochloric acid aqueous solution was poured into the system until white floccus precipitation emerged. Then **3** was obtained as a yellow-green solid (1.76 g, yield 85.64%) after the liquid was filtered away and the precipitation was dried in a vacuum chamber at 40 ℃ for 12 h [^{1}H NMR (dimethyl sulfoxide-d_6) δ: 8.44 (s, 1H), 8.25 (s, 2H), 7.47−7.68 (m, 6H), 6.95 (d, J=8.8 Hz, 2H), 3.98 (t, J=6.8 Hz, 2H), 1.66−1.72 (m, 2H), 1.13−1.31 (m, 18H), 0.83 (t, J=7.2 Hz, 3H); ^{13}C NMR (dimethyl sulfoxide-d_6) δ: 166.3, 159.7, 136.1, 133.6, 132.5, 131.9, 130.5, 123.9, 115.4, 70.2, 68.1, 56.5, 31.8, 29.5, 29.2, 25.9, 22.6, 14.4. MALDI-TOF, m/z: calcd 550.3; found 550.3 (M^+)]. Finally, the OPE amphiphile (**4**) was synthesized according to the following route: **3** (20 mg), *N*-(3-dimethylaminopropyl)-*N'*-ethylcarbodiimide hydrochloride (EDC•HCl) (60 mg), *N*-hydroxysuccinimide (NHS) (36 mg), and poly(ethylene glycol) bis(3-aminopropyl) terminated (diamino PEG) (M_n≈1500) (0.3272 g) were dissolved in 20 mL of DMF. And the resulting mixture was stirred at room temperature for 74 h. Thereafter, the resulting mixture was purified by dialysis against water for 3 d with a dialysis bag (MWCO=3500 Da) to remove the excess EDC•HCl, NHS, DMF and diamino PEG. The product was then obtained as loose-yellow powder by freeze drying for 2 d (0.11 g). ^{1}H NMR ($CDCl_3$) δ: 8.16, 7.49, 6.87 (the chemical shift of benzene ring), 5.30 (NH_2), 3.97 (Ph-O-CH_2), 3.64 (PEG chain), 1.26 (alkyl chain). GPC analysis: M_w=7389, M_n=6622, and polydispersity distribution index (PDI) is 1.12. To synthesize anion OPE amphiphile (**5**), 0.15 g **3** was concentrated in a methyl amine solution (25%−30 wt% water). The residual methyl amine was then removed via rotary evaporation and the remaining salt was obtained by freeze drying.

Self-assembly of 4 in water

Appropriate amount of **4** was dissolved in deionized water to prepare three bottles of solution with different concentrations: 0.0642, 0.1297, and 0.2168 mg/mL. After ultrasonic treatment for 10 min, the mixtures were stirred vigorously for another 24 h. The light-cloudy solution obtained was then filtered through 0.22 μm size filter membrane for further investigation. Hollow nanospheres were prepared through aging the solution (0.2168 mg/mL) for one week at room temperature.

Results and Discussion

Synthesis and structure characterization

The preparation process of OPE amphiphile (**4**) is shown in Scheme 1. Particularly, the preparation of **2** was accomplished via Sonogashira reaction in the mixture of diisopropylamine solution in the presence of $Pd(PPh_3)_4$/CuI catalyst at 85 ℃ for 24 h. This "one-pot" reaction to synthesize asymmetric OPE conjugated molecular provided a rapid and convenient approach of asymmetric synthesis with a relatively high yield. Actually, more efforts have been made to prepare **2** through "step-by-step" reaction, however, a quite low yield (about 10%) was obtained owing to the complex reaction process. Subsequently, **3** was prepared through hydrolysis reaction and then acid treatment. After the activation of the carboxylic groups on **3** with EDC•HCl and NHS, diamino PEG was linked to **3** via the amidation reaction. It is worth noting that large excess of diamino PEG ($n_{\text{diamino PEG}}$ ∶ n_3=6 ∶ 1) was used to make it possible that only one amino group of diamino PEG can be employed rather than formation of large crosslinking. However, GPC analysis indicated the formation of crosslinking with about three OPE backbone units. Additionally, anion OPE amphiphile (**5**) was easily obtained under alkali treatment. The correct structure of all the products was confirmed by NMR, GC-MS, MALDI-TOF and GPC analysis.

The existence of free amino groups could be determined by ^{1}H NMR spectra (Figure 1). **4** exhibited a distinct peak at δ 5.3 when the solvent was $CDCl_3$ (Figure 1c). Interestingly, this specific peak disappeared after adding a drop of CH_3OD into the solution (Figure 1b), which can be attributed to the replacement of hydrogen atoms corresponding to NH_2 by deuterium atom of

CHINESE JOURNAL OF CHEMISTRY

Scheme 1 The preparation process of oligo(*p*-phenyleneethynylene) amphiphiles (**4** and **5**)

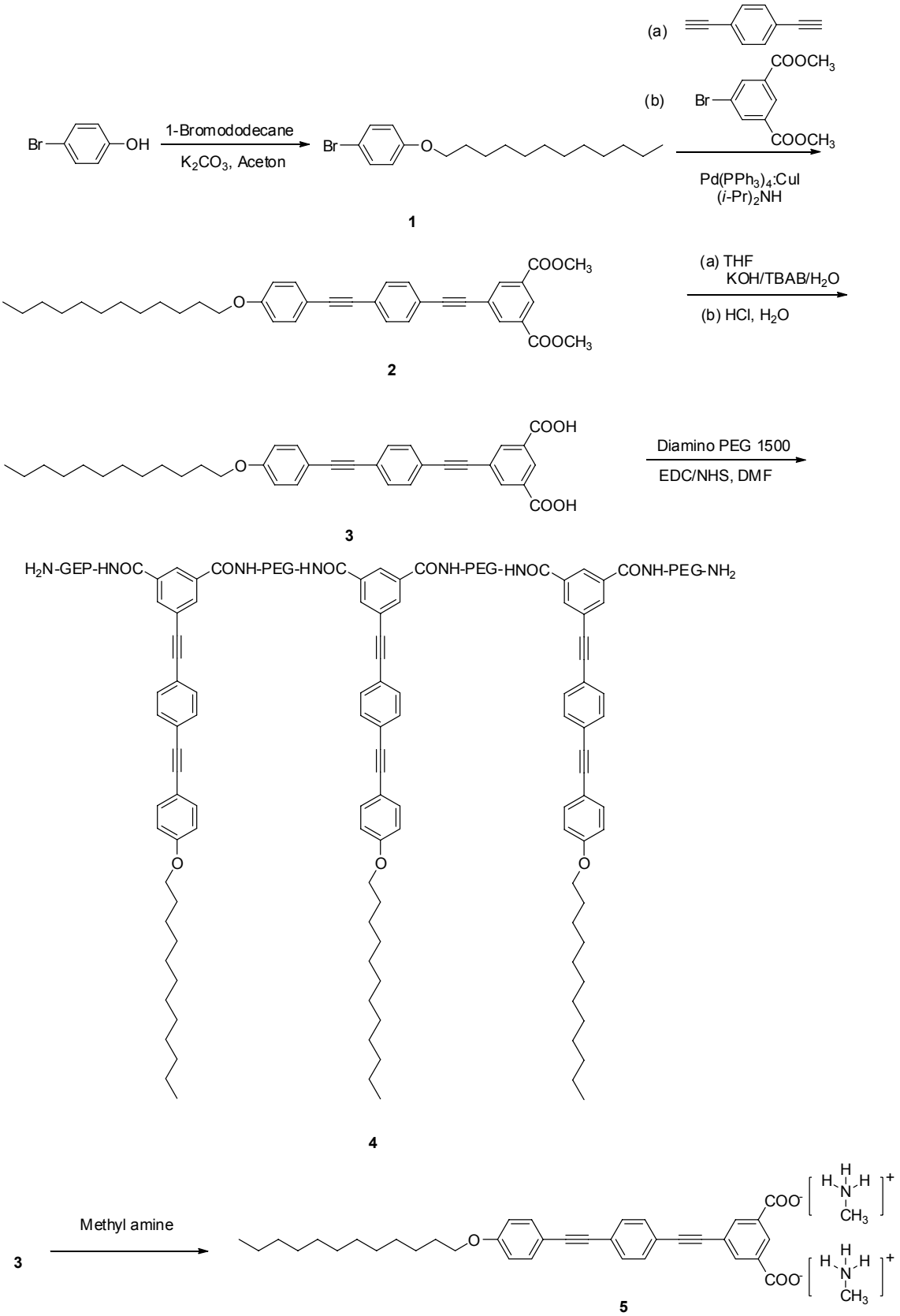

CH_3OD for the activity of amino group. Furthermore, when **4** was reconstituted into D_2O, specific peaks of OPE and alkyl chains disappeared at their proton spectra while only the specific peaks of PEG were shown (Figure 1a). These results indicated that OPE and alkyl chain were condensed in the core and PEG chains acted

as the outstretched shell, which strongly confirmed the formation of nanoparticles while the OPE amphiphile was reconstituted in water.[26]

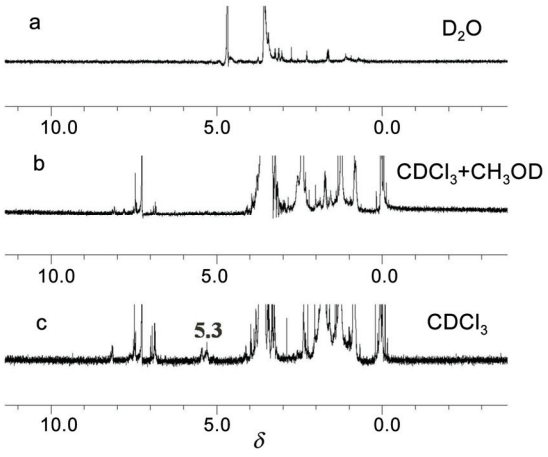

Figure 1 ^{1}H NMR of **4** in different solvents (D_2O, $CDCl_3$ and $CDCl_3$+CH_3OD).

The covalent linkage of diamino PEG to **3** was further confirmed by FT-IR spectrometry (Figure 2). The absorption peak at 1725 cm^{-1} in Figure 2b is attributed to the carboxylic carbonyl groups of **3** (C=O stretching) which is absent in Figure 2c. Yet a new peak at *ca.* 1657 cm^{-1} has arised that can be assigned to the amide carbonyl groups. This provided reasonable evidence that diamino PEG was successfully linked to **3** by amidation reaction. Different from the previous literature report,[27] the carboxyl groups of **3** have disappeared completely in our product for the superfluous diamino PEG we used. Besides, the FT-IR spectrum of **4** showed a strong band at 1112 cm^{-1} attributed to the stretching vibration of ether bond (C—O—C) of PEG chains, which further confirmed the successful modification of diamino PEG to **3**.

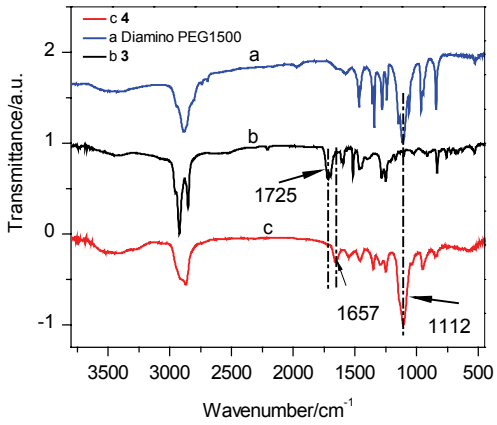

Figure 2 FT-IR of **4**, **3** and diamino PEG 1500.

Photophysical properties

The UV-vis and photoluminescence spectra of **4** and **5** with the same concentration of 0.1 mg/mL in different solvents were shown in Figure 3. In tetrahydrofuran (THF) solution, **4** exhibited a strong absorption peak occurring at 330 nm with a vibronic band shoulder at 351 nm and a tail absorption band at 388 nm (Figure 3d). Similar situation has occured to **4** in aqueous solution (Figure 3d), which also exhibited a strong absorption peak at 330 nm. However, an enhanced tail absorption band at 388 nm was observed in comparison with that in THF. Furthermore, the concentration dependent absorption spectra of **4** in water were detected in Figure S2, which indicated a gradually increasing trend of the tail absorption band with the concentration ranging from 0.05 to 0.25 mg/mL. Correspondingly, the photoluminescence peak maximum of **4** in water appeared at 454 nm with the concentration of 0.1 mg/mL, which was beyond 47 nm red shift from the emission in THF (Figure 3b). All these optical properties revealed the typical J-type aggregation[28,14] of **4** in aqueous solution. Figure 3c demonstrated the absorption band of **5** in water and THF, and the most striking feature is that the vibronic band shoulder at 351 nm of **5** in THF is much stronger than that of **4** (Figure 3d). Besides, a slight bathochromic shift happened from **4** to **5** with about 10 nm in emission spectra in THF (Figure 3a and Figure 3b), and all of these indicated that the conjugated segments of **5** may have a strong tendency to form interchain aggregates[29] for its weaker solubility than **4** in THF. It can be hypothesized that carboxylic acid ions (COO^-) enhanced the polarity and inorganic nature of **5**, which can not be dissolved very well in THF.

Interestingly, almost the opposite results were obtained in aqueous solution. In comparison with **4**, the absorption (Figure 3c) and emission (Figure 3a) peaks of **5** presented obvious blue-shift. This possibly resulted from the mutual repulsion among the negative charges (COO^-) leading to a more twisted main chain conformation, and hence a decreased effective conjugation length.[30] The abovementioned results also supported that adjusting relative proportion of hydrophilic-hydrophobic parts would play effective roles to control photophysical properties as well as the aggregation states of amphiphilic conjugated molecules.

Morphological and superficial properties

Like a host of amphiphilic molecules, **4** contains distinct hydrophobic and hydrophilic segments, which would undergo self-assembly in aqueous solution to form diversified structures. To intuitively investigate the morphology of OPE nanoparticles, fluorescence microscopy and TEM measurements were carried out. Fluorescence micrograph of **4** in water was shown in Figure 4, which presented that the nanoparticles which emitted vivid blue light were dispersed well in aqueous solution, and Brownian motion of the nanoparticles can also be seen clearly. To explore the representative results of self-assembly, three bottles of aqueous solution with different concentrations (0.0642, 0.1297, and

CHINESE JOURNAL OF CHEMISTRY

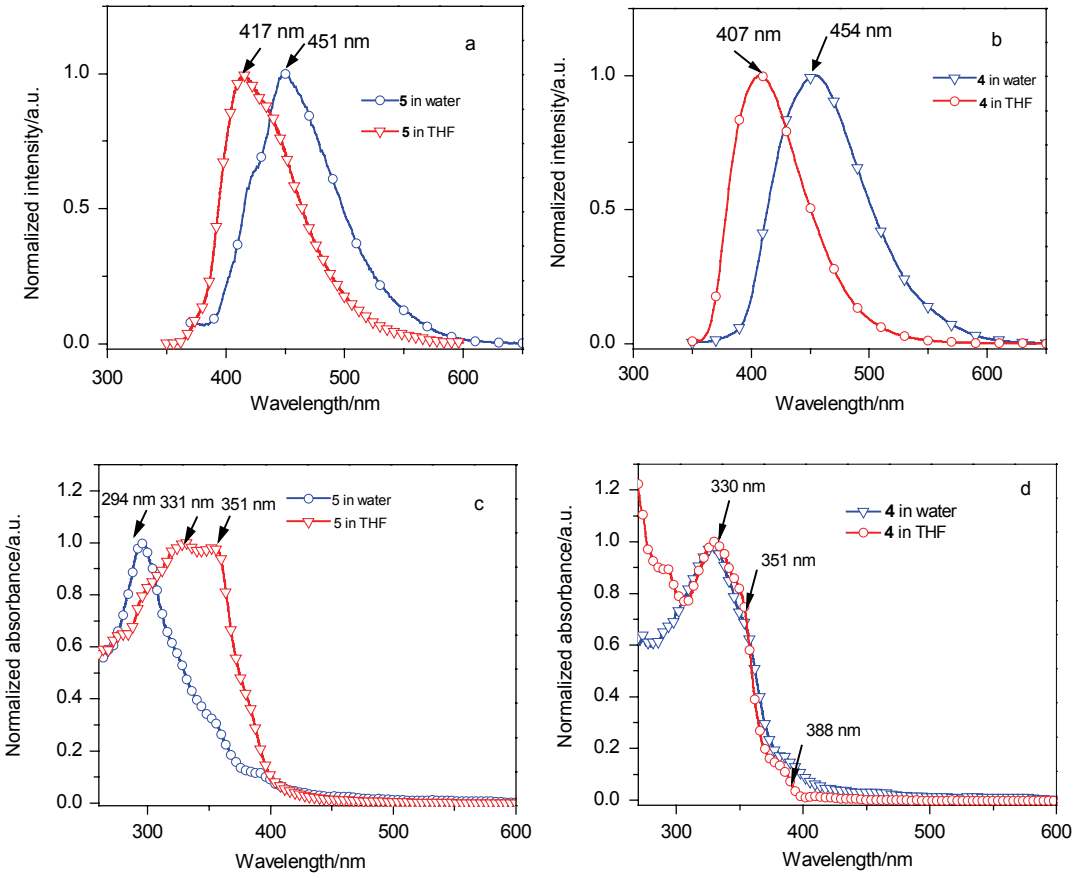

Figure 3 UV-vis (c and d) and photoluminescence spectra (a and b) of **4** and **5** in different solvents (0.1 mg/mL). The excited wavelength of emission spectra was fixed at 340 nm.

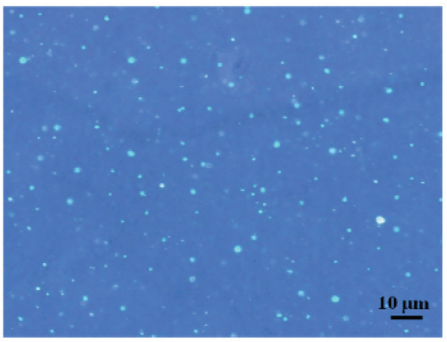

Figure 4 Representative fluorescence micrograph of the nanoparticles formed by self-assembly of **4** in water.

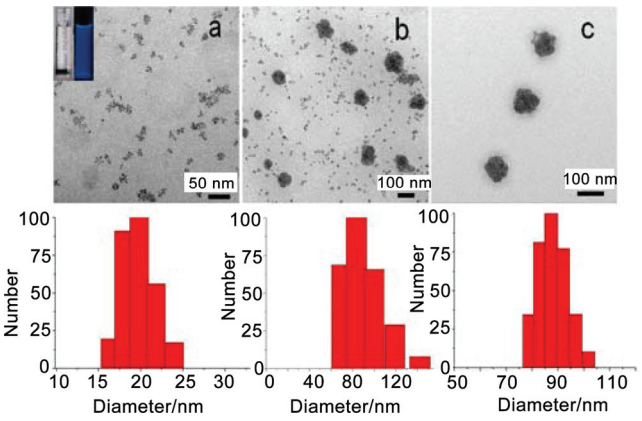

Figure 5 TEM images and hydrodynamic diameter distribution of the nanoparticles in different morphologies (a, 0.0642 mg/mL; b, 0.1297 mg/mL; c, 0.2168 mg/mL). Inset: photographs of the nanoparticles aqueous solution (left) under ambient light and (right) under a black lamp (λ=365 nm).

0.2168 mg/mL) were employed. It is worth noting that the data we chose were based on the photoluminescence spectra of **4** with various concentrations (Figure S1), which indicated that continuous increase of fluorescence intensity of **4** in water has been observed with the concentration varying from 0.01 mg/mL to 0.1297 mg/mL, yet a decrease with the concentration changing from 0.1297 mg/mL to 0.2845 mg/mL. Figure 5 showed the TEM images and hydrodynamic diameter distribution of the nanoparticles with different morphologies. In Figure **5a** (c=0.0642 mg/mL), the nanoparticles with a clear grain-like structure were observed with a diameter of (10±1.2) nm, which was a little smaller than DLS result (mean diameter: 19.6 nm). This is probably attributed to the stretch of PEG chains in aqueous solution while shrink after dried on a copper grid coated with a carbon film. With the concentration increased to 0.2168 mg/mL (Figure 5c), strawberry-like nanoparticles appeared with a diameter of (93±2.2) nm which was in

accordance with the DLS result (mean diameter: 93.5 nm). Naturally, both the two kinds of aggregation morphology can be observed in a middle-concentration, such as 0.1297 mg/mL (Figure 5b). Interestingly, through aging the solution (0.2168 mg/mL) for 3 d, irregular nanostructure formed spontaneously (Figure 6a), which further evolved into uniform hollow nanospheres (Figure 6b) after one week. Based on these, we hypothesized that monodisperse single nanoparticles (similar with nanomicelles) can be formed by self-assembly process at a low concentration of 0.0642 mg/mL firstly, and subsequently, with the increase of amphiphilic OPE concentration from 0.1297 to 0.2168 mg/mL, large aggregates would be constructed from single nanoparticles,[14] and their sizes sharply increased to *ca.* 93.5 nm (DLS result). However, these aggregates are not stable enough, which would crimp (see arrows indicated region in Figure 6a) to form more stable nanostructures through aging the solution for 3 d. And finally, hollow nanospheres were spontaneously constructed (Figure 6b) after one week, which may result from high thermodynamics and kinetics stability of these hollow nanostructures. The possible self-assembly process of the nanoparticles was shown in Scheme 2. Therefore, we provided a facile access to tuning morphology and size of nanostructures without complicated procedures, such as changing solvent environments and adjusting molecular structures. Compared with **4**, no uniform morphology was observed when **5** was dispersed in water for its low water-solubility.

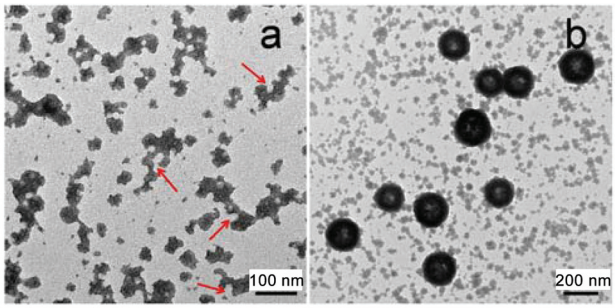

Figure 6 TEM images of the OPE nanoparticles aged for 3 d (a) and one week (b) at room temperature (c=0.2168 mg/mL).

As we know, surface charge of nanoparticles plays a vital role in biological system such as preventing rapid nonspecific uptake *in vivo*[27] and binding biomolecules.[31] Therefore, the surface charge properties of the hollow nanospheres (Figure 7a) and the irregular aggregates formed by **5** (Figure 7b) were studied respectively by measuring the zeta potentials as a function of pH values. As shown in Figure 7, b exhibited negative potentials in the pH range from 4.00 to 9.18, and the zeta potential became more negative with the increase of pH values, which can be attributed to the gradual ionization of carboxylic groups on the surface of nanoparticles. By contrast, hollow nanospheres exhibited positive potentials when pH values were adjusted below 9.18, resulting from the protonation of the amino groups. Fortunately, the nearly neutral surface of nanospheres in physiological environments (pH≈7.4) would lead to a longer blood circulation due to their weak electrostatic interaction with proteins in comparison to the charged nanoparticles.[27]

Scheme 2 Schematic of the possible formation process of the hollow nanospheres

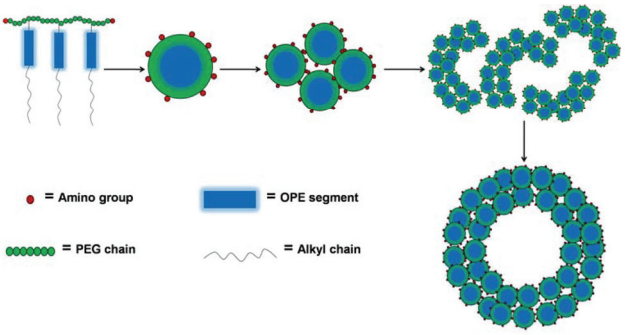

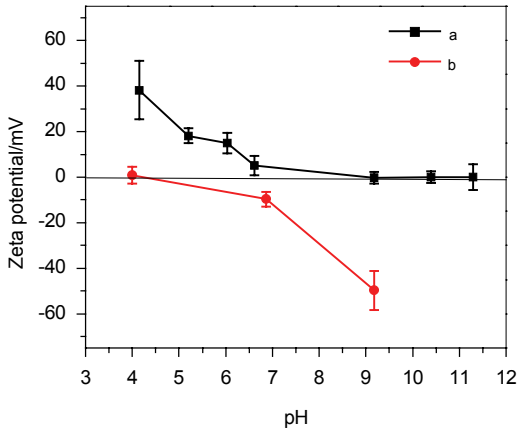

Figure 7 pH-dependent zeta potential curves of hollow nanospheres (a) and the irregular aggregates formed by **5** (b).

Cellular viability and imaging

To evaluate the potential biomedical applications of OPE nanoparticles, their biocompatibility to PANC-1 cells was also assessed by an MTT assay. Figure 8 summarized the viability of PANC-1 cells cultured with the OPE amphiphile (**4**) aqueous solution at different concentrations ranging from 0.0001 mg/mL to 0.5 mg/mL for 24 h. It is clearly observed that all the cells presented high viability (>90%) after treating with the OPE nanoparticles with different concentrations. The influences of OPE nanoparticles to PANC-1 cells were also examined by investigating the cellular morphology at different time nodes (0 h and 24 h) using optical microscopy (Figure S3). As shown in Figure S3, cells still adhered to the plate very well and no obvious cell morphology change was observed after they were incubated with OPE nanoparticles (0.5 mg/mL) for 24 h. All of these proved the low cytotoxicity of OPE nanoparticles, which provided large possibility for cellular imaging or

other biological applications.

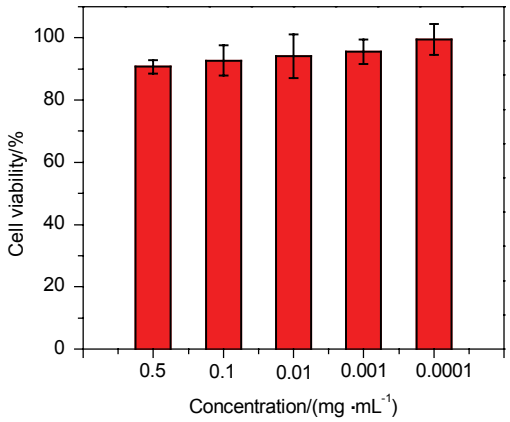

Figure 8 *In vitro* cell viability graph of **4** with different concentrations by MTT assay.

Figure 9 showed the *Z*-scan measurement for **4** dissolved in methanol (0.1 mg/mL), which indicated a two-photon absorption (2PA) feature. The 2PA cross-section, δ, can be estimated according to the following formula:

$$\delta = h\nu\beta/N$$

N is the number of molecules per cm^3 and $h\nu$ is the photon energy.

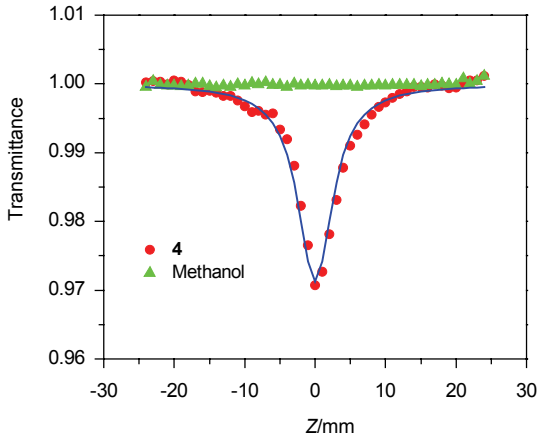

Figure 9 *Z*-scan signature for 4-methanol solution (0.1 mg/mL, scatters) performed with 190 fs pulses at 720 nm. The solid lines represent theoretical fittings with the parameters obtained in the experiments.

Given that **4** exhibited exactly high 2PA cross-section (δ was calculated to 1181 GM in methanol with laser excitation at 720 nm), we set out to demonstrate that our material could be used for intracellular imaging. Two-photon excited live cell imaging using **4** was investigated with confocal laser scanning microscopy coupled to a Coherent MIRA Ti: sapphire laser. After 24 h of incubation with the hollow nanospheres solution of **4** (0.2168 mg/mL), the cells were washed three times in PBS buffer. The excitation wavelength was fixed at 720 nm. As seen in Figure 10(b), a strong fluorescence from the cellular cytoplasm was observed and it was clear that the 2PFM images provided considerably high contrast and spatial resolution. All of these demonstrated that our material can be employed as an efficient fluorescent probe for two-photon cell imaging, which provided opportunities for long-term imaging with reduced photodamage in comparison with UV-excited imaging.[32]

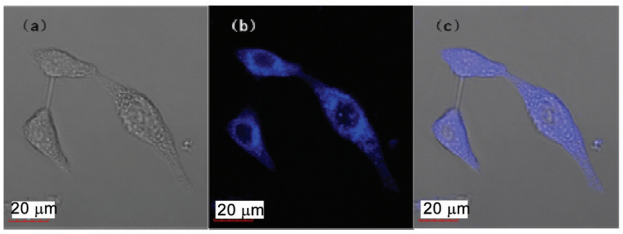

Figure 10 Two-photon images of PANC-1 cells treated with the hollow nanospheres solution of **4** (0.2168 mg/mL). Two-photon microscopy images were obtained with laser excitation at 720 nm.

Conclusions

In summary, a novel fluorescent water-soluble amphiphilic oligomer based on PEG and OPE was firstly reported. In aqueous solution, this material can spontaneously self-assemble into nanoparticles with the size ranging from 19.6 to 93.5 nm along with the morphology change from "grain" to "strawberry" just through adjusting concentration of the solution. After the solution was aged for one week, homogeneous hollow nanospheres were spontaneously constructed. These results provided a facile approach to tuning morphology and size of self-assembled nanostructures. The morphology and size of nanoparticles were characterized by TEM, fluorescence microscope and DLS, and their photophysical properties were also investigated. Good water-solubility, low cytotoxicity and exactly high 2PA cross-section made our material an excellent candidate as a two-photon sensitizer and a new class of probe for bioimaging using 2PFM. Besides, this kind of nanospheres may act as carriers of drug or inorganic material such as magnetic nanoparticles (MNPs) and gold nanoparticles (GNPs) to form multifunctional nano-probes. A more comprehensive study of employing the nanospheres as templates to fabricate multifunctional nanomaterials is of great significance. More excitingly, abundant amino groups on particle surface make it available for subsequent modifications, which would endow the OPE nanoparticles more powerful functions in specific probing, multimodal imaging and multimodal therapy in biomedical field.

Acknowledgement

This work was financially supported by the National Basic Research Program of China (Nos. 2012CB933301

and 2012CB723402), the Ministry of Education of China (No. IRT1148), the National Natural Science Foundation of China (Nos. 61378081, 21222404, 51173080 and 21104033) and the Innovation Program for Ordinary Higher Education Graduate of Jiangsu Province of China (No. KYLX_0796), Synergetic Innovation Center for Organic Electronics and Information Displays and the Natural Science Foundation of Jiangsu Province of China (Nos. BZ2010043, NY211003, BM2012010).

References

[1] Thomas, S. W.; Joly, G. D.; Swager, T. M. *Chem. Rev.* **2007**, *107*, 1339.
[2] Fan, L. J.; Zhang, Y.; Murphy, C. B.; Angell, S. E.; Parker, M. F. L.; Flynn, B. R.; Jones, W. E. *Coord. Chem. Rev.* **2009**, *253*, 410.
[3] Li, K.; Liu, B. *Polym. Chem.* **2010**, *1*, 252.
[4] Sun, P. F.; Fan, Q. L.; Liu, L. L.; Deng, W. X.; Lu, X. M.; Huang, W. *Acta Polym. Sin.* **2014**, *12*, 1629.
[5] Zhu, C.; Liu, L.; Yang, Q.; Lv, F.; Wang, S. *Chem. Rev.* **2012**, *112*, 4687.
[6] Jiang, R. C.; Lu, X. M.; Yang, M. H.; Deng, W. X.; Fan, Q. L.; Huang, W. *Biomacromolecules* **2013**, *14*, 3643.
[7] Liong, M.; Angelos, S.; Choi, E.; Patel, K.; Stoddart, J. F.; Zink, J. I. *J. Mater. Chem.* **2009**, *19*, 6251.
[8] Wu, C.; Szymanski, C.; McNeill, J. *Langmuir* **2006**, *22*, 2956.
[9] Pecher, J.; Mecking, S. *Chem. Rev.* **2010**, *110*, 6260.
[10] Dey, S.; Sreenivasan, K. *J. Mater. Chem. B* **2015**, *3*, 824.
[11] Park, S. J.; Kang, S. G.; Fryd, M.; Saven, J. G.; Park, S. J. *J. Am. Chem. Soc.* **2010**, *132*, 9931.
[12] Yuan, Y.; Liu, J.; Liu, B. *Angew. Chem.* **2014**, *126*, 7291.
[13] Lu, X. M.; Fan, Q. L.; Zhang, G. W.; Pu, K. Y.; Huang, W. *Sci. China Chem.* **2010**, *53*, 1122.
[14] Yin, C.; Song, W. L.; Jiang, R. C.; Lu, X. M.; Hu, W. B.; Shen, Q. M.; Li, X.; Li, J.; Fan, Q. L.; Huang, W. *Polym. Chem.* **2014**, *5*, 5598.
[15] Wu, C.; Chiu, D. T. *Angew. Chem., Int. Ed.* **2013**, *52*, 3086.
[16] Ringsdorf, H.; Schlarb, B.; Venzmer, J. *Angew. Chem., Int. Ed.* **1988**, *27*, 113.
[17] Wang, C.; Wang, Z.; Zhang, X. *Acc. Chem. Res.* **2012**, *45*, 608.
[18] Pu, K. Y.; Li, K.; Shi, J. B.; Liu, B. *Chem. Mater.* **2009**, *21*, 3816.
[19] Li, K.; Pu, K. Y.; Cai, L. P.; Liu, B. *Chem. Mater.* **2011**, *23*, 2113.
[20] Zhang, G. W.; Lu, X. M.; Wang, Y. Y.; Huang, Y. Q.; Fan, Q. L.; Huang, W. *Polym. Int.* **2011**, *60*, 45.
[21] Ryu, J.; Lee, M. *J. Am. Chem. Soc.* **2005**, *127*, 14170.
[22] Moon, K.; Kim, H.; Lee, E.; Lee, M. *Angew. Chem., Int. Ed.* **2007**, *46*, 6807.
[23] Moon, K.; Lee, E.; Lee, M. *Chem. Commun.* **2008**, 3061.
[24] Photos, P. J.; Bacakova, L.; Discher, B.; Bates, F. S.; Discher, D. E. *J. Control. Release* **2003**, *90*, 323.
[25] Clark, A. P. Z.; Shen, K. F.; Rubin, Y. F.; Tolbert, S. H. *Nano Lett.* **2005**, *5*, 1647.
[26] Kim, D. G.; Jeong, Y. I.; Choi, C.; Roh, S. H.; Kang, S. K.; Jang, M. K.; Nah, J. W. *Int. J. Pharm.* **2006**, *319*, 130.
[27] Liu, D.; Wu, W.; Ling, J.; Wen, S.; Gu, N.; Zhang, X. *Adv. Funct. Mater.* **2011**, *21*, 1498.
[28] Ajayaghosh, A.; Varghese, R.; Praveen, V. K.; Mahesh, S. *Angew. Chem., Int. Ed.* **2006**, *45*, 3261.
[29] Tan, C.; Pinto, M. R.; Schanze, K. S. *Chem. Commun.* **2002**, 446.
[30] Fan, Q. L.; Zhou, Y.; Lu, X. M.; Hou, X. Y.; Huang, W. *Macromolecules* **2005**, *38*, 2927.
[31] Hong, R.; Fischer, N. O.; Emrick, T.; Rotello, V. M. *Chem. Mater.* **2005**, *17*, 4617.
[32] Yong, K. T.; Qian, J.; Roy, I.; Lee, H. H.; Bergey, E. J.; Tramposch, K. M.; He, S.; Swihart, M. T.; Maitra, A.; Prasad, P. N. *Nano Lett.* **2007**, *7*, 761.

(Zhao, X.)

